PMASynRM late design-stage rotor shape NVH optimization

Sebastian Ciceo[*,†,‡], Fabien Chauvicourt[*], Bogdan Varaticeanu[§], Johan Gyselinck[†] and Claudia Martis[‡]
[*]Engineering Services RTD, Siemens Industry Software NV, Leuven, Belgium, Email: sebastian.ciceo@siemens.com
[†]BEAMS Department, Electrical Energy Group, Université Libre de Bruxelles, Brussels, Belgium
[‡]Department of Electrical Machines and Drives, Technical University of Cluj-Napoca, Cluj-Napoca, Romania
[§]Servomotors Department, ICPE, Bucharest, Romania

***Abstract*—Electrical machine electromagnetic-caused noise and vibration represents an ever-increasing target for machine-designers. A novel late design-stage NVH optimization method using the full rotational velocity synthesized vibration-response map is proposed. This is assisted by a target-setting method for the most important force harmonics using a force sensitivity analysis. The procedure is applied on a PMASynRM used for light traction applications, where the rotor cross-section is modified by introducing notches and saliency. The results for different percentages of permitted decrease in average show that both resonances and individual frequency orders can be directly targeted and minimized.**

***Index Terms*—PMASynRM, design optimization, NVH, electromagnetic forces, vibration-synthesis, structural-dynamics, vibration, notches.**

I. Introduction

The accelerating market push for automotive electrification and advanced driver-assistance systems (ADAS) gives electrical machine designers stricter Noise, Vibration and Harshness (NVH) design targets. The absence of the masking combustion-engine broadband noise amplifies the annoyance perception caused by the electric powertrain, tire-road interaction and wind noise. This, together with the electromagnetic, thermal and structural requirements, makes the design and optimization of electrical machine a complex multi-disciplinary, multi-physics problem [1].

We can distinguish between two noise-mitigating optimization approaches for electrical machine design defined by the design-cycle positioning: the early-stage approach where the design space is the same for every domain target and NVH requirements are competing with the other multi-physics requirements [2], [3] and the late-stage approach where all other targets except NVH are satisfied and only minor modifications to the machine cross-section are allowed, where usually a trade-off has to be made between electromagnetic and NVH requirements [4], [5]. For the early-stage method it is easier to find a global solution with respect to a multi-attribute cost function, but the NVH transfer path (structure and air-born) has a higher degree of uncertainty in comparison with the late-design stage where usually the transfer path is better known thus making vibro-acoustic results more reliable.

In this paper two novel procedures, based on the vibration-synthesis introduced by Boesing [6] allowing for fast vibro-acoustic simulations, that assist the late-design stage optimization process are introduced:

- An air-gap force harmonics sensitivity analysis presented in Section II-B, with the purpose of establishing a cause-effect relationship between a specific force harmonic and the overall vibration response of the electrical machine. The method allows to set-up NVH optimization cost functions based on force harmonics before modifying the machine cross-section. This brings an improvement to the state of the art, where usually the geometrical modifications are introduced first and the effects on the forces and vibration response are analyzed afterwards at one or a few numbers of RPM operating points [4], [7]–[10].
- Using synthesized run-up spectrograms as metrics in the design space exploration process in order to assist the machine-designer when selecting the optimal design on the full RPM-frequency range.

The machine under study is a Permanent-Magnet Assisted Synchronous Reluctance Machine (PMASynRM) with the parameters detailed in Table I and was designed for light traction application with low-cost ferrite permanent magnets, with additional construction details given in [11]. One operating point was used in the optimization process: $i_d = -60A$ and $i_q = 100A$ and the amplitude of the vibration response in all presented results is scaled. The mechanical transfer path is represented by the stator structure but this can be easily extended to the full powertrain structure, including boundary conditions.

II. PMASynRM magneto-mechanical coupling

A. Structural dynamics analysis using vibration synthesis

The forced response of the stator structure is computed using the vibration synthesis method. The first step in the process is the orthogonal decomposition (cos-sin) of the air-gap force pressure ($f_{rad,tan}(t, \alpha)$, where t represents time and α is the air-gap position), in both radial and tangential directions, followed by the superposition of the most impor-

TABLE I
3-PHASE 6-POLE PMASYNRM PARAMETERS [11]

Parameter	unit	value
Rated voltage	V	100
Rated current amplitude	A	101
Base speed	rpm	2100
Maximum speed	rpm	9000
Stator outer diameter	mm	170
Rotor outer diameter	mm	114
Stator stack length	mm	110
Air gap length	mm	0.5

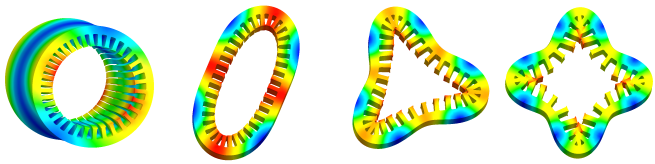

(a) (b) (c) (d)

Fig. 1. Significant stator mode shapes: (a) Mode 0 at 8287Hz, (b) Mode 2 at 946Hzm, (c) Mode 3 at 2545Hz and (d) Mode 4 at 4589Hz.

tant space orders (m):

$$f_{rad,tan[sup]}(t,\alpha) = f_{rad,tan[DC]}(t) + \sum_{m=1}^{M}(f_{rad,tan[cos,m]}(t)cos(m\alpha) + f_{rad,tan[sin,m]}(t)sin(m\alpha)). \quad (1)$$

The vibration is calculated numerically in Simcenter 3D as the superposition of dynamic responses excited by each significant force shape. This is achieved with a modal frequency response solution, having the excitation $F_{[I],shape}$ a unitary force shape where the total energy per frequency line is equal to 1 N [12]:

$$v_{[I],shape}(f) = H(f)F_{[I],shape}(f), \quad (2)$$

where $v_{[I],shape}(f)$ is the frequency response for each force shape excitation and $H(f)$ is the transfer function obtained from modal analysis (stator mode shapes together with their eigenfrequencies are presented in Figure 1). The unitary frequency response for an air-born NVH significant mesh node (in both radial and tangential direction) for the most important force shapes (again both radial and tangential components) for the machine under test are presented in Figure 2.

The total response $v(f)$ is the superposition of all frequency responses scaled with the cos-sin frequency domain amplitude factors obtained from Equation 1:

$$v(f) = v_{[I],DC}(f)f_{DC}(f) + \sum_{m=1}^{M}(v_{[I],cos_m}f_{cos,m}(f) + v_{[I],sin_m}f_{sin,m}(f)). \quad (3)$$

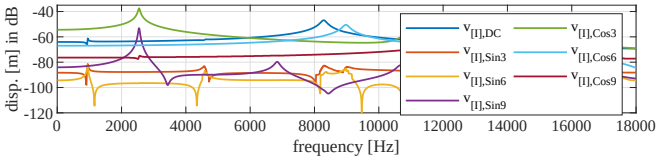

(a) radial direction response for radial unitary force excitation

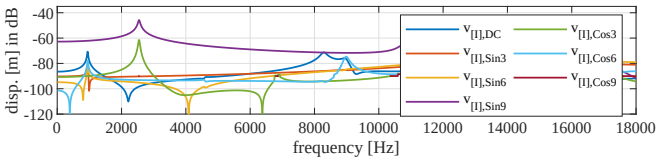

(b) tangetial direction response for radial unitary force excitation

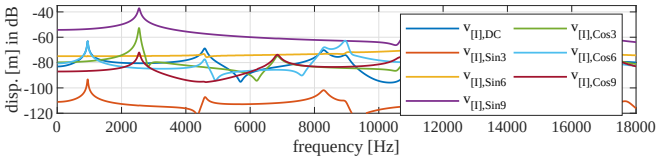

(c) radial direction response for tangetial unitary force excitation

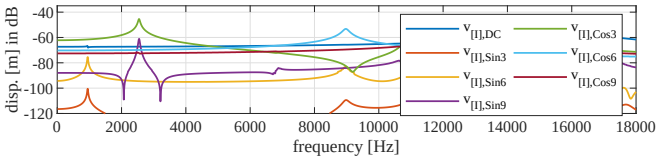

(d) tangetial direction response for tangential unitary force excitation

Fig. 2. Displacement for unitary frequency responses.

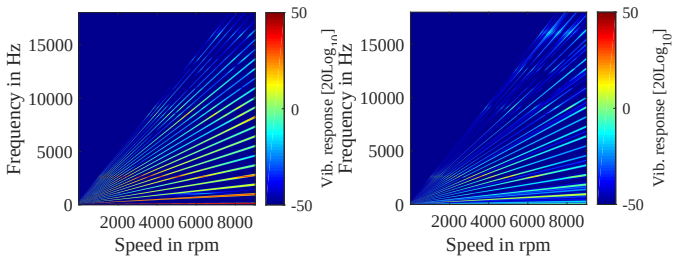

(a) radial direction (b) tangential direction

Fig. 3. Synthesized stator vibration response spectrograms using both the radial and tangential force components.

This method allows for fast computation of full-RPM range run-up spectrograms as presented in Figure 3.

B. Force harmonics sensitivity analysis based on the vibration synthesis

In order to determine which force harmonics have an important impact on the final vibration response, a sensitivity analysis is performed. This is accomplished by subtracting the time and space force excitation ($F_{rad,tan[time,space]}$) from the computation of the total response and directly analyzing the effects on the run-up spectrogram:

$$\Delta v_{-F_{rad,tan[time,space]}}(f,\omega) = v_0(f,\omega) - v_{-F_{rad,tan[time,space]}}(f,\omega), \quad (4)$$

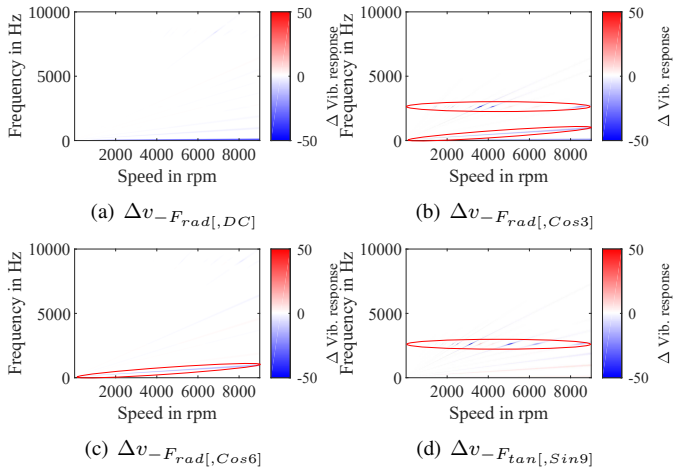

Fig. 4. Synthesized stator vibration response (radial direction) force sensitivity analysis.

where $\Delta v_{-F_{rad,tan[time,space]}}(f,\omega)$ is the difference between the baseline spectrogram $v_0(f,\omega)$ containing all force excitation and $v_{-F_{rad,tan[time,space]}}(f,\omega)$ representing the spectrogram without the specific time and space force excitation factor.

Results for the spatial force factors, including all temporal components, that have an important impact on the vibration spectrogram are presented in Figure 4. We observe that by completely removing one-by-one the force harmonic components from the computation of the final response there are specific components that are more influential than others, where: $F_{rad[6,Cos3]}$ and $F_{rad[6,Cos6]}$ have a significant impact on the first frequency order-cut while $F_{rad[36,Cos3]}$, $F_{rad[42,Cos3]}$, $F_{tan[24,Sin9]}$, $F_{tan[30,Sin9]}$ and $F_{tan[48,Sin9]}$ interact with the 3^{rd} mode at 2545 Hz causing resonance. The resonance-causing force shapes can also be identified from the unitary frequency responses (Figure 2), but without having information on the specific frequency orders and response amplitude.

III. Electrical Machine NVH Optimisation

A. Rotor shape modification

In order to change the desired force harmonics, the following design variables are introduced: rotor saliency depth Δg, a d-axis circular rotor notch defined by the radius r_1 and an elliptical rotor notch defined by the major radius r_2, minor radius r_3 and angle β, as presented in Figure 5.

B. Defining the optimization problem

The cost function for the optimization problem is defined on the basis of the force harmonics determined in Section II-B. The linear weights for each individual force harmonic is set in the following way: 50% is attributed for the first frequency order causing force harmonics $F_{rad[6,Cos3]}$ and $F_{rad[6,Cos6]}$, with w_{t1} and w_{t2} and 50% is attributed for the resonance-causing force harmonics $F_{rad[36,Cos3]}$, $F_{rad[42,Cos3]}$, $F_{tan[24,Sin9]}$, $F_{tan[30,Sin9]}$ and $F_{tan[48,Sin9]}$

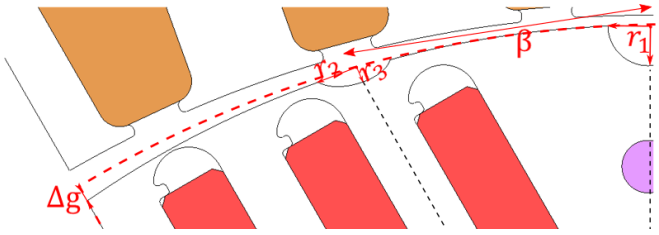

Fig. 5. Rotor shape modification used in the optimization process with the original structure showed with a (red dotted line).

with w_{r1}, w_{r2}, w_{r3}, w_{r4} and w_{r5}. Each individual weight is determined using the vibration response force sensitivity analysis and represents a weight in function of the local minimum of vibration displacement reduced by each individual force shape and the global minimum. The cost function has the following form:

$$f_0 = w_{t1}\frac{F_{rad[6,Cos3]}}{F_{rad[6,Cos3],baseline}} + w_{t2}\frac{F_{rad[6,Cos6]}}{F_{rad[6,Cos6],baseline}} + w_{r1}\frac{F_{rad[36,Cos3]}}{F_{rad[36,Cos3],baseline}} + w_{r2}\frac{F_{rad[42,Cos3]}}{F_{rad[42,Cos3],baseline}} + w_{r3}\frac{F_{tan[24,Sin9]}}{F_{tan[24,Sin9],baseline}} + w_{r4}\frac{F_{tan[30,Sin9]}}{F_{tan[30,Sin9],baseline}} + w_{r4}\frac{F_{tan[48,Sin9]}}{F_{tan[48,Sin9],baseline}}. \quad (5)$$

The inequality constraints are defined as a function of the baseline average torque times a relaxation factor: $c_1 = r \cdot T_{average,baseline}$) and the baseline torque ripple times the inverse of the relaxation factor (before continuous stator skewing is applied): $c_2 = (1/r) \cdot T_{ripple,baseline}$. The optimization problem is stated as follows:

$$\begin{aligned} &\text{minimize} \quad f_0 \\ &\text{subject to} \quad c1 \leq T_{average} \,\&\, T_{ripple} \leq c2. \end{aligned}$$

The hybrid adaptive algorithm SHERPA from Simcenter HEEDS was chosen to perform the optimization routine because of its proven efficiency and robustness [13], where 150 evaluations are performed for 3 different values of torque relaxation factors: $r = 0.975$, $r = 0.95$ and $r = 1$.

IV. Optimization Results

For the case where $r = 1$, where no decrease in average torque is permitted, we can observe in Figure 6 a strong correlation between $T_{average}$ and the first frequency order causing force harmonics $F_{rad[6,Cos3]}$, $F_{rad[6,Cos6]}$. We observe that an increase in average torque leads to an increase in the amplitude of the force factors and consequently in the vibration-response amplitude increase of the first frequency order.

The final selected optimal designs for the 3 different r-valued cases are presented in Figure 7. Results for the design variables for $r = 0.95$ are: $\Delta g = 6.09$, $r_1 = 0.49$, $r_2 = 1.02$,

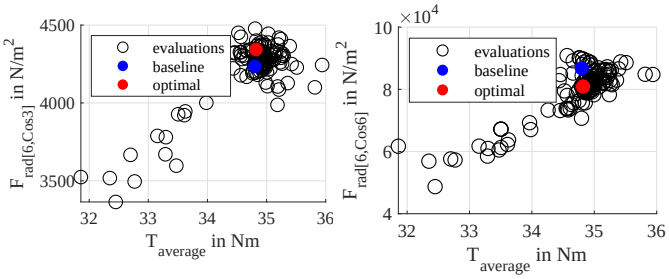

Fig. 6. Correlation between $T_{average}$ and $F_{rad[6,Cos3]}$ (a) and $F_{rad[3,Cos3]}$ (b).

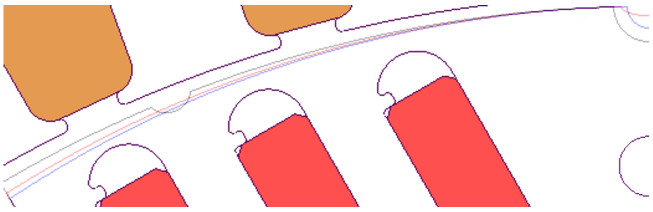

Fig. 7. Selected optimized designs for $r = 1$ (black), $r = 0.975$ (red) and $r = 0.95$ (blue).

$r_3 = 0.79$ and $\beta = 27.9$, for $r = 0.975$: $\Delta g = 4.34$, $r_1 = 0.4$, $r_2 = 1.11$, $r_3 = 0.4$ and $\beta = 0.1$ and for $r = 1$: $\Delta g = 0.91$, $r_1 = 1.54$, $r_2 = 0.89$, $r_3 = 0.61$ and $\beta = 21.62$. We can observe that the torque relaxation factor is inversely correlated with the rotor saliency depth.

The results for the force harmonics used in the cost functions are presented in Figure 8. Except for the hard-constrained case of $r = 1$ where $F_{rad[6,Cos3]}$ and $F_{tan[30,Sin9]}$ were not reduced with respect to the baseline values, all other force harmonics decreased in amplitude.

The torque waveform results are presented in Figure 9. As an indirect consequence of reducing the target force harmonics, the peak-to-peak torque is reduced by 3% for

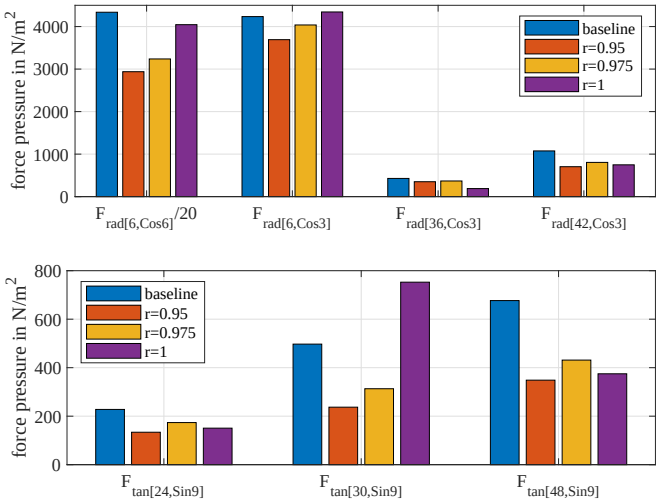

Fig. 8. Force harmonics for the baseline and optimized designs.

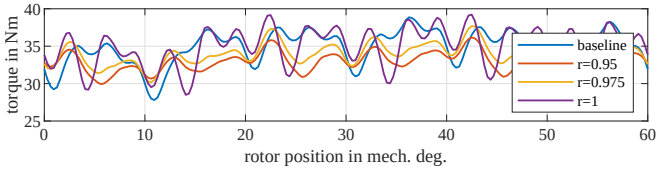

Fig. 9. Instantaneous rotor-position dependent torque for the baseline and optimized designs.

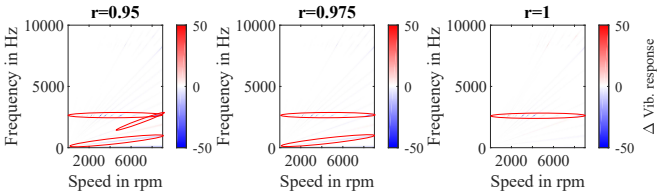

Fig. 10. Absolute difference between the baseline and optimized design in the stator vibration response spectrograms for the 3 torque relaxation factors.

$r = 1$, 32% for $r = 0.975$ and 42% for $r = 0.95$.

The vibration response is again assessed using the vibration-synthesis method on the full RPM-frequency range, the absolute difference in vibration response between the original and optimized designs are shown in Figure 10. We observe that gains obtained by reducing the vibration response amplitude are decreased at a torque relaxation factor closer to 1. Order cuts for different multiples of the base mechanical frequency are presented in Figure 11, where a considerable decrease in the vibration response for each order can be observed, the exception of $f = 12f_{mech}$. This does not represent an issue, because the maximum amplitude of this frequency order is significantly lower compared to rest of the orders. The hard-constrained case of $r = 1$ also underperforms the baseline case for order 24 and 30.

V. Conclusions

Electrical machine vibro-acoustic optimization is becoming an important task for machine-designers. This paper proposes a process that includes the full run-up vibration spectrogram as a design metric and gives force harmonics targets for the optimization cost function. This process is applied to a low-cost PMASynRM where the rotor is modified in order to shape the air-gap radial and tangential forces. For the first order-cut ($f = 6f_{mech}$) the following improvements in vibration response values ($[20Log_{10}]$ scale) are found: 1.2% for $r = 1$, 5.8% for $r = 0.975$ and 8.95% for $r = 0.95$, while for the most significant resonant-causing order cut ($f = 48f_{mech}$) the values are: 11.3% for $r = 1$, 9% for $r = 0.975$ and 13.7% for $r = 0.95$ (giving-up 5% of the average torque).

The method can be extended to multiple operation points that may include drive-cycles and control strategies such as Maximum Torque Per Ampere. Also, different cost functions, such as torque ripple and iron losses can be introduced in the multi-objective optimization procedure and stress analysis should be performed on the new rotor geometry.

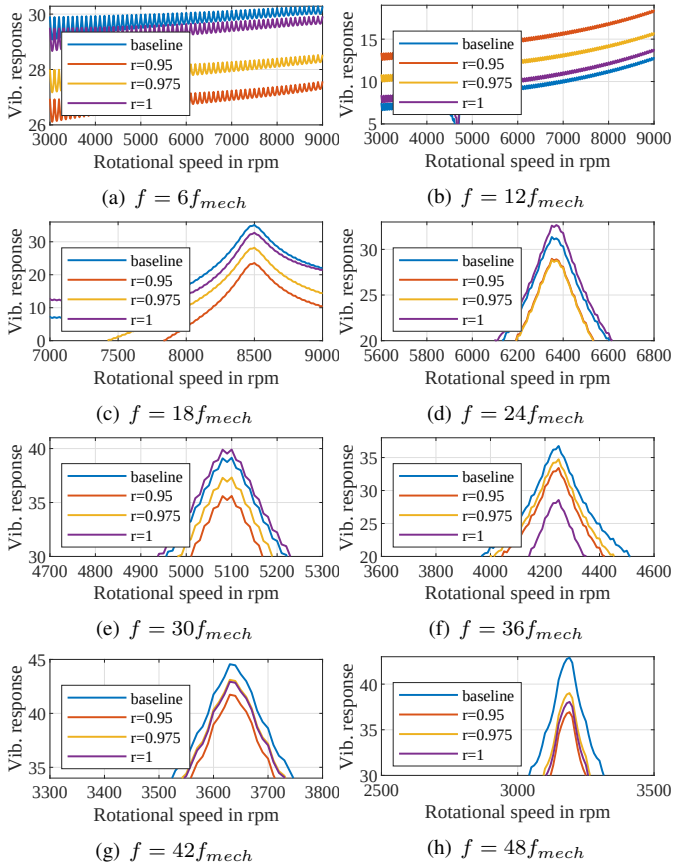

Fig. 11. Vibration displacement ($[20Log_{10}]$ scale) order-cuts for different multiples of the base mechanical rotation frequency for the baseline and optimized designs.

VI. Acknowledgment

This paper is part of the European Industrial Doctorate on Next Generation for sustaINable auTomotive ElectRical ACtuaTion (INTERACT) project which has received funding from the European Union Horizon 2020 research and innovation programme under grant agreement No 766180. Sebastian Ciceo is an Early Stage Researcher on this project. The authors also would like to acknowledge JSOL Corporation for granting access to JMAG software packages.

References

[1] G. Bramerdorfer, J. A. Tapia, J. J. Pyrhönen, and A. Cavagnino, "Modern electrical machine design optimization: Techniques, trends, and best practices," *IEEE Transactions on Industrial Electronics*, vol. 65, no. 10, pp. 7672–7684, 2018.

[2] M. Mohammadi, T. Rahman, R. Silva, B. Wang, K. Chang, and D. Lowther, "Effect of acoustic noise on optimal synrm design regions," *IEEE Transactions on Magnetics*, vol. 54, no. 3, pp. 1–4, 2017.

[3] I. Ibrahim, M. Mohammadi, V. Ghorbanian, and D. A. Lowther, "Effect of pulsewidth modulation on electromagnetic noise of interior permanent magnet synchronous motor drives," *IEEE Transactions on Magnetics*, vol. 55, no. 10, pp. 1–5, 2019.

[4] A. Andersson and T. Thiringer, "Electrical machine acoustic noise reduction based on rotor surface modifications," in *2016 IEEE Energy Conversion Congress and Exposition (ECCE)*. IEEE, 2016, pp. 1–7.

[5] J. Nägelkrämer, A. Heitmann, and N. Parspour, "Multi-objective optimization of the rotor design to improve the acoustic behavior of high power density interior permanent magnet synchronous machines," in *Stuttgart*, 2017.

[6] M. Boesing, T. Schoenen, K. A. Kasper, and R. W. De Doncker, "Vibration synthesis for electrical machines based on force response superposition," *IEEE Transactions on Magnetics*, vol. 46, no. 8, pp. 2986–2989, 2010.

[7] J. Krotsch and B. Piepenbreier, "Radial forces in external rotor permanent magnet synchronous motors with non-overlapping windings," *IEEE Transactions on Industrial Electronics*, vol. 59, no. 5, pp. 2267–2276, 2011.

[8] G.-Y. Zhou and J.-X. Shen, "Rotor notching for electromagnetic noise reduction of induction motors," *IEEE Transactions on Industry Applications*, vol. 53, no. 4, pp. 3361–3370, 2017.

[9] Z. Wu, Y. Fan, H. Wen, and D. Gao, "Vibration suppression of fscw-ipm with auxiliary slots," in *2018 IEEE Energy Conversion Congress and Exposition (ECCE)*. IEEE, 2018, pp. 3222–3227.

[10] Q. Wang, J. Li, R. Qu, and Y. Lu, "Design and optimization of a permanent magnet synchronous machine for low vibration and noise applications," in *2018 21st International Conference on Electrical Machines and Systems (ICEMS)*. IEEE, 2018, pp. 280–284.

[11] B. Varaticeanu, P. Minciunescu, and S. Matei, "Performance evaluation of permanent magnet assisted synchronous reluctance motor for micro electric vehicle," in *Advanced Microsystems for Automotive Applications 2015*. Springer, 2016, pp. 173–186.

[12] F. Chauvicourt, S. Ciceo, and H. Van der Auweraer, "On the use of vibration synthesis to ease electric machine powertrain design," in *2019 IEEE International Electric Machines & Drives Conference (IEMDC)*. IEEE, 2019, pp. 1118–1125.

[13] N. Chase, M. Redemacher, E. Goodman, R. Averill, and R. Sidhu, "A benchmark study of optimization search algorithms," *Red Cedar Technology, MI, USA*, pp. 1–15, 2010.

VII. Biographies

Sebastian Ciceo obtained his M.Sc in Electrical Engineering from the Technical University of Cluj-Napoca in 2017. He currently works at Siemens PLM Software, Leuven as an Early-stage researcher (ESR) in the frame of the H2020 MSCA EID 2017-2021 research project INTERACT. He is pursuing a joint PhD degree with Université Libre de Bruxelles and the Technical University of Cluj-Napoca. He's main research interest are: model-based system engineering and testing, electrical machines and drives, electrical mobility, structural dynamics,multibody dynamics, multi-physics optimization and control.

Fabien Chauvicourt obtained a double PhD degree in Mechanical Engineering from KU Leuven (Belgium) and Engineering Science and Technology from Université Libre de Bruxelles (Belgium). He is currently a research engineer at Siemens PLM Software, Leuven. His domains of interest are: mechatronic systems, structural dynamics, multi-attribute simulation and testing of electric drives and vehicles, electric mobility (e-cars, e-aircrafts, e-drones), machine learning, innovative concept designs for more sustainable world, biomimetics.

Bogdan Varaticeanu obtained his PhD degree in Electrical Engineering from the University Politehnica of Bucharest (Romania), in 2012. During 2014 and 2015 he followed a postdoctoral internship at University Politehnica of Bucharest. He is currently a research engineer at ICPE, Servomotors Department. His main domains of interest are: electromagnetic and thermal design of special electrical machines, rotors integrity design for high-speed electric motors, electric mobility, numerical modelling of electromagnetic fields and additive manufacturing.

Johan Gyselinck obtained his M.Sc. and PhD degree in electromechanical engineering from the Ghent University (Belgium) in 1991 and 2000 respectively. From 2000 till 2004 he was postdoctoral researcher and lecturer at the University of Lige (Belgium). Since 2004 he is professor at the Université Libre de Bruxelles (ULB, Belgium). His main teaching and research topics are low-frequency magnetics (finite-element and analytical modelling, numerical methods), electrical machines and drives (modelling, simulation, design and experimental work), and renewables (wind and photovoltaics). He is (co-)author of some 300 journal and conference papers.

Claudia Martis graduated with a MsC in Electrical Engineering and a PhD degree in Electrical Engineering from Technical University of Cluj-Napoca, Romania, in 1990 and 2001 respectively. Since 1996 she is member of the teaching staff of the Faculty of Electrical Engineering at Technical University of Cluj-Napoca. She is currently Professor with the Department of Electrical Machines and Drives of the same university and her research is focused on electrical machines and drives design, modeling, analysis and testing for automotive, renewable energy-based and industrial applications.